ELECTRONIC SUPPLEMENTARY INFORMATION

Ammonia Borane Assisted Mechanochemical Boost of Electrochemical Performance of Basal Planes of MoS_2-Type Materials

February 2, 2023

S1 Experimental details

S1.1 Materials

Molybdenum(IV) sulfide MoS_2 (99 %), molybdenum(IV) selenide $MoSe_2$ (99.9 %) and tungsten(IV) sulfide WS_2 (99.8 %) are purchased from Alfa Aesar, while ammonia borane NH_3BH_3 (97 %, further in the text ABH) is purchased from Boron Specialties.

Molybdenum(IV) telluride $MoTe_2$, tungsten(IV) telluride and tungsten(IV) selenide WSe_2 were prepared by overnight heating of molybdenum (Koch Light Labs, 99.99 %) or tungsten (Koch Light Labs, 99.99 %) with stoichiometric amount of tellurium (Alfa Aesar, $2-5$ mm shots, 99.9999 %) or selenium (Alfa Aesar, $2-5$ mm shots, 99.999 %) at 900 °C in evacuated quartz tube.

S1.2 Exfoliation

Samples are prepared as listed in Table S1. Since the Raman spectra and XRD patterns show that the most successful intercallation of ABH was achieved for the graphite : ABH = 1 : 2.7 mass ratio (Fig. S2), the analogous procedure was then applied to exfoliate TMDCs by ABH, by taking into account the difference of molecular mass of TMDCs formula units with respect of graphite (where formula unit is C), in order to reproduce molar ratio.

A Spex 8000M mill-shaker was used for preparations of the samples for further characterization. Milling frequency was 875 cycles per minute in a figure eightshape motion, and the applied milling time was 30 min. In all preparations, the mass of reaction mixture was ≈ 250 mg. In-house designed gas-tight mechanochemical jars (Fig. S1) were made of Böhler N685 Extra stainless steel,[1] which is CNC machined and hardened by thermal treatment by Mitar Ltd. This steel was chosen due to its hardness and high chemical inertness. All the mechanochemical treatments were done in these jars with 1 stainless steel ball $m = 4$ g.

To ensure inert atmosphere during the milling of the samples, all manipulations were conducted in an argon-filled Labmaster 130 MBRAUN glovebox (< 0.1 ppm O_2 and < 0.1 ppm H_2O).

Table S1: Preparation of the samples.

Sample	Abbr.	$m(MX_2)$/mg	m(ABH)/mg	total mass (mg)	ABH : MX_2
graphite + ABH		38	273	311	2.7 : 1
MoS_2	MoS2	200	—	200	—
MoS_2 + ABH	MoS2-ABH	150	202	352	7.0 : 1
$MoSe_2$	MoSe2	256	—	256	—
$MoSe_2$ + ABH	MoSe2-ABH	110	200	310	7.0 : 1
$MoTe_2$	MoTe2	170	—	170	—
$MoTe_2$ + ABH	MoTe2-ABH	233	153	386	7.5 : 1
WS_2	WS2	230	—	230	—
WS_2 + ABH	WS2-ABH	96	202	298	8.2 : 1
WSe_2	WSe2	245	—	230	—
WSe_2 + ABH	WSe2-ABH	150	100	250	7.4 : 1
WTe_2	WT2	245	—	230	—
WTe_2 + ABH	WT2-ABHA	200	118	318	8.4 : 1

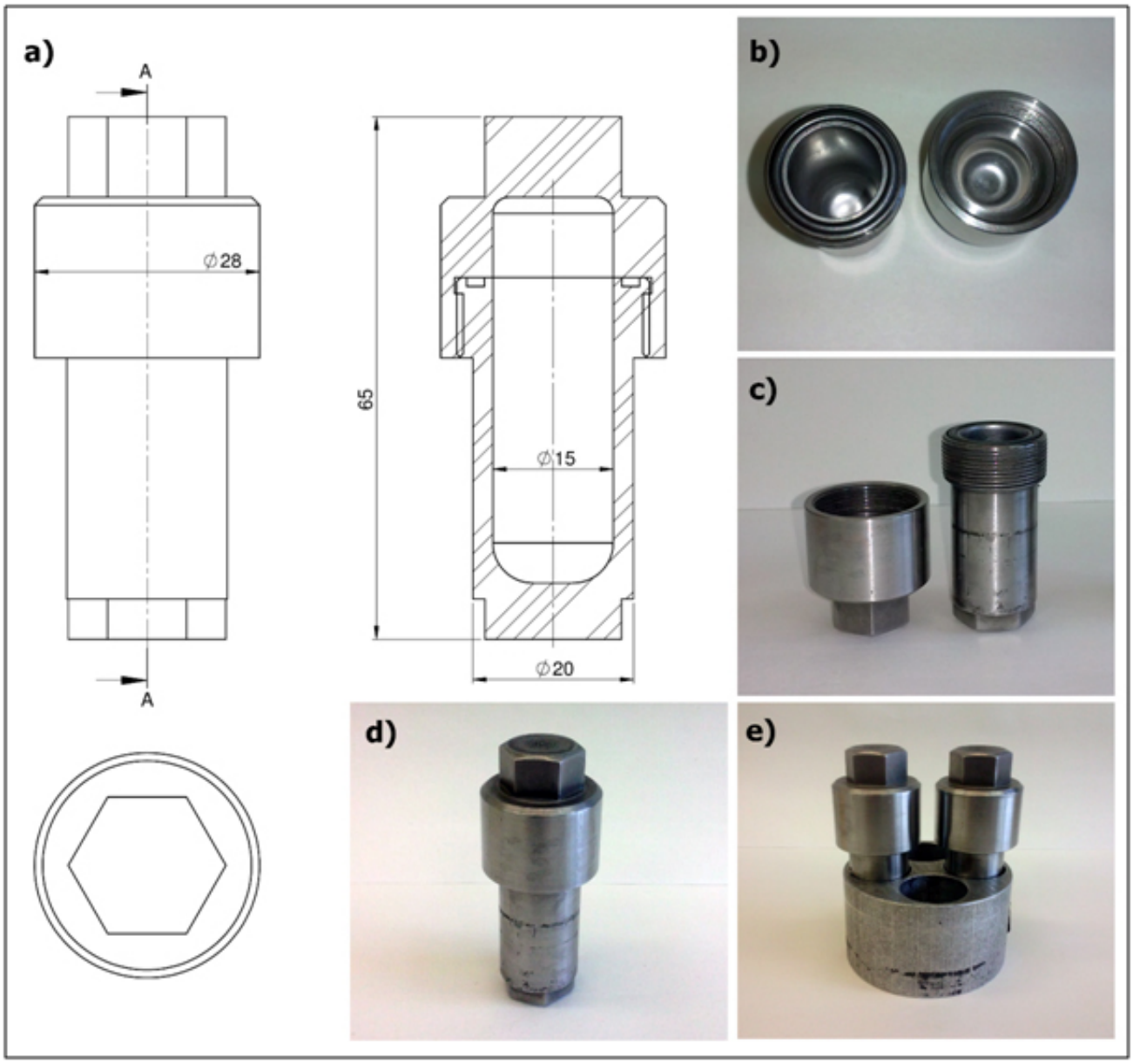

Figure S1: Home-made stainless steel milling jar: a) technical drawing; b) interior of clean jar; c) opened jar prepared for sample loading; d) closed jar; e) two jars in SPEX sample holder prepared for mounting on the mill.

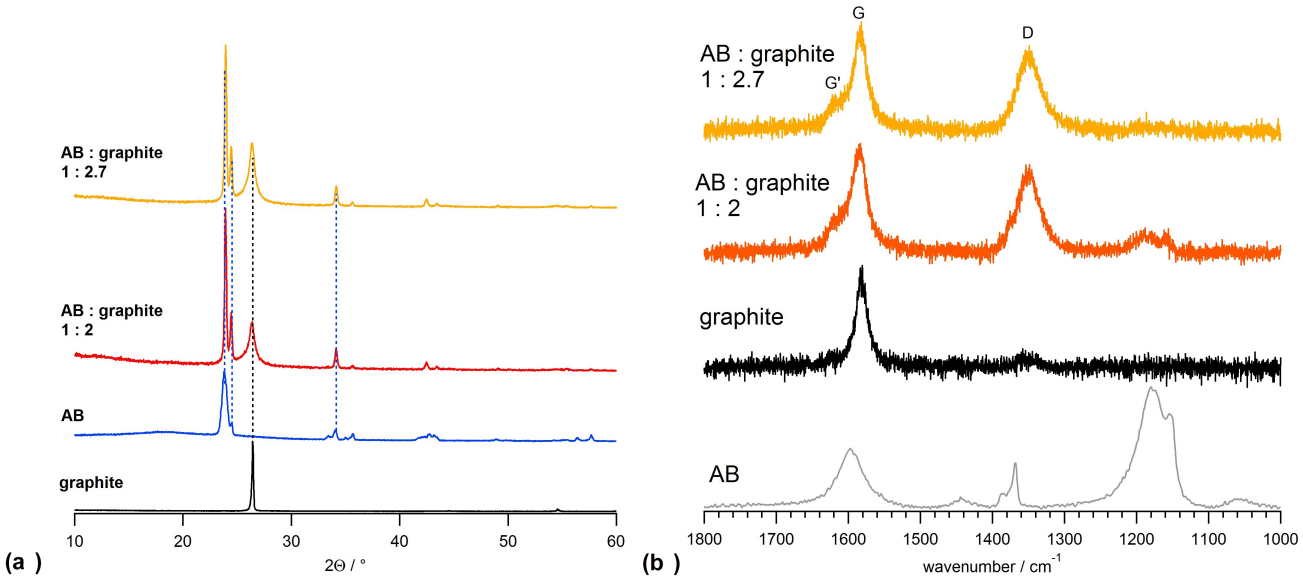

Figure S2: XRD patterns (a) and Raman spectra (b) of pristine ABH and graphite and post-milled samples of ABH + graphite mixtures with ABH : graphite weight ratio 1 : 2 and 1 : 2.7, milled over 2×90 min (to be compared with Fig. 1 of ref.[2]).

S1.3 Characterisation

X-ray diffraction powder patterns (PXRD) were recorded using a Panalytical Aeris system with CuKα radiation ($\lambda = 1.5418$ Å). The 2Θ range was $5 - 70°$ with a $\Delta(2\Theta) = 0.0221°$ step and counting time per step was 0.25 s. Average crystal thickness along a specific plane (in this case (002) for thickness and (110) for lateral size of the flakes) was determined using Scherrer's relation:

$$\tau_{hkl} = \frac{K\lambda}{\beta \cos \Theta}$$

where K is a dimensionless shape constant of the crystal (usually 0.9), λ is the wavelength of applied X-rays, β is full width at half height and Θ is the scattering angle of the corresponding reflection. The number of exfoliated layers was obtained by dividing the average thickness by the unit cell length.

Infrared (IR) spectra in ATR mode are measureed by a ABHB Bomem MB102 FTIR spectrometer with DTGS detector and CsI optics, equipped with a Specac Golden Gate single-reflection ATR accessory with type IIIA diamond trigonal-prism shaped ATR element metal-bonded into a tungsten carbide mount. The angle of incidence is 45°. This optical assembly enables acquisition of IR spectra in $4000 - 450\,\mathrm{cm}^{-1}$ range. Each spectrum represents an average of 10 co-added Fourier-transformed interferograms (scans). The nominal resolution is $4\,\mathrm{cm}^{-1}$ which gives a distance between two points in the resulting spectrum $2\,\mathrm{cm}^{-1}$.

Temperature-dependant IR spectra are acquired in transmission mode, using KBr pellets (~ 100 mgKBr : $sim1$ mgsample). The controlled heating of the samples was allowed by use of Specac's high-stability temperature controller. The samples were continuously heated from room emperature to 250 °C at a heating rate $5\,^{\circ}\mathrm{C\,min}^{-1}$, and the spectra were acquired at a 5 °C step. Spectral resolution was set to $4\,\mathrm{cm}^{-1}$, and each spectrum represents an average of 5 co-added Fourier-transformed interferograms (scans), which took 10 s per spectrum, implying temperature accuracy of ±1 °C.

Thermogravimetric analysis coupled with quadrupole mass spectroscopy (QMS-TG) was done using a Netzsch STA 449F5 instrument. 85 µL Al_2O_3 crucibles with drilled lids were used as a sample holders. Heating rate was set to $5\,^{\circ}\mathrm{C\,min}^{-1}$. N_2 was used for both purging ($20\,\mathrm{mL\,min}^{-1}$) and protective gas ($50\,\mathrm{mL\,min}^{-1}$). The measurements were done over a $35 - 700\,^{\circ}\mathrm{C}$ temperature range. Gaseeous products over a $1 - 100$ au mass range were measured by a QMS coupled to TG through a 2 m long capillary tube heated to 250 °C to prevent condensation.

UV-vis spectra were recorded using a Cary 50 spectrometer. For spectroscopic measurements, samples in ethanol (GramMol, 96 %) were sonicated for in a Bandelin Sonorex ultrasonic bath over 30 min.

Particle size distribution was measured by dynamic light scattering (DLS), using a Malvern Zetasizer Nano ZS, which measures ζ-potential in liquid dispersions, in the hydrodinamic size range between 0.6 nm and 6 µm. Samples were dispersed by sonication over 30 min in petroleum ether as liquid matrix.

Scanning electron microscope (SEM) with energy dispersive X-ray spectroscopy (EDS) measurements were done using a FEG Quanta 250 SEM FEI and a Jeol 7000 FE-SEM instrument.

X-ray photoelectron spectra (XPS) were measured using a Specs XPS instrument fitted with an XR-50 dual anode X-ray source and a Phoibos 150 energy analyzer. The powdered samples were pressed onto an indium foil

Table S2: Experimental conditions for exfoliations of TMDCs and sample naming ('t' states for individual milling time).

MX_2		MX_2 + ABH		milling time (min)
system	name	system	name	
MoS_2	MoS2-t	MoS_2 + ABH	MoS2-ABH-t	480
$MoSe_2$	MoSe2-t	$MoSe_2$ + ABH	MoSe2-ABH-t	450
$MoTe_2$	MT-t	$MoTe_2$ + ABH	MoTe-ABH-t	180
WS_2	WS2-t	WS_2 + ABH	WS2-ABH-t	300
WSe_2	WSe2-t	WSe_2 + ABH	WSe2-ABH-t	360
WTe_2	WTe2-t	WTe_2 + ABH	WTe-ABH-t	270

for mounting. The Al K_α X-ray source with 150 W (14 kV) was employed for the measurements. The spectra were acquired with a step size of 0.1 eV and a pass energy of 20 eV with 25 scans.

The electrocatalytic activity of the prepared both pristine and mechanochemically treated samples has been measured by linear sweep voltammetry (LSV), using an Ivium Vertex.One potentiostate/galvanostate. The measurements have been carried out in the conventional three-electrode cell setup with 1 moldm^{-3} aqueous solution of H_2SO_4 as electrolyte. Graphite plate and SCE (saturated calomel electrode, SI Analytics) were used as counter and reference electrode, respectively. Working electrode consisted of the active material and polyvinylidene-difluoride (PVDF, Sigma-Aldrich) mixed in 95 : 5 wt. ratio and deposited on a glassy carbon plate from the slurry prepared in *N*-methyl-2-pyrrolidone (Sigma-Aldrich 99 %).

Test for NH_3: a filter paper was soaked by 1 mol dm^{-3} aqueous solution of $CuCl_2$. Contact with NH_3 results in formation of dark blue complex:

$$Cu^{2+} + 4\,NH_3 + 2\,H_2O \longrightarrow [Cu(NH_3)_4(H_2O)_2]^{2+}$$

S2 Consideration of mechanical exfoliation

Understanding of the complex mechanics of the processes occuring inside the milling jar is still limited. However, the available literature[3–6] enables at least a qualitative description of exfoliation process.[7,8]

In this study, we use a SPEX 8000M mill-shaker. This is a vibratory mill, which agitates the vial at a high frequency in a complex three-axis cycle. The center of vial vibrates in 2D mode with the same frequency, but with different amplitude. The main axis of the vial is slanted and it rotates (at the same frequency) around the axis of precession. One or more balls, and their mutual colisions, as well as colisions with the inner wall of the vial, induced by the movement of the vial, thus transferring the mechanical energy to the reaction mixture, represent a driving force of mechanochemical process.

Generally, inside the layers of lamellar materials, atoms are in strong covalent interaction. On the other hand, the interaction between layers is weak van der Waals. Thus, layers easily slip one over the others, which is reflected in characteristic low effective coefficients of friction, making these materials good solid lubricants.

S3 ABH-assisted exfoliation of graphite

In order to check out the applicability of the Spex 8000M mill-shaker for exfoliations, we repeated the previously published ball milling ABH-assisted exfoliation of graphite, which was done in a planetary mill.[2]

Raman spectra and PXRD patterns of the obtained samples (Fig. S2) are equal to those published by Liu et al. It is also concluded that the optimal results in given conditions are obtained for ABH : graphite = 1 : 2.7 weight ratio.

S4 Exfoliation of transition metal dichalcogenides (TMDC)

First, PXRDs of pristine TMDCs are given in Fig. S3. On the first sight, it is visible that the position of (002) line, that reflects the interlayer separation in the bulk crystal is mainly determined by dichalcogenide, rather than metal atoms, i.e. interlayer distance in MoS_2 and WS_2 are very similar etc. The position of this line is determined by ionic radius of dichalcogenide atoms. They are linearly correlated, as seen from Fig. S4.

Two series of TMDC exfoliations by ball milling were done. First, the samples of neat MX_2 (M = Mo, W; X = S, Se, Te) were milled in stainless steel jars in argon; second, the samples of MX_2 + ABH mixtures were milled in the same conditions. Samples and their naming are listed in table S2.

PXRD patterns of the pristine (bulk), *ex-situ* monitored and final samples are given in Figs. S5 - **??**. It is clear that milling of the neat MX_2 results is amorphisation of the sample, visible from significant broadening of

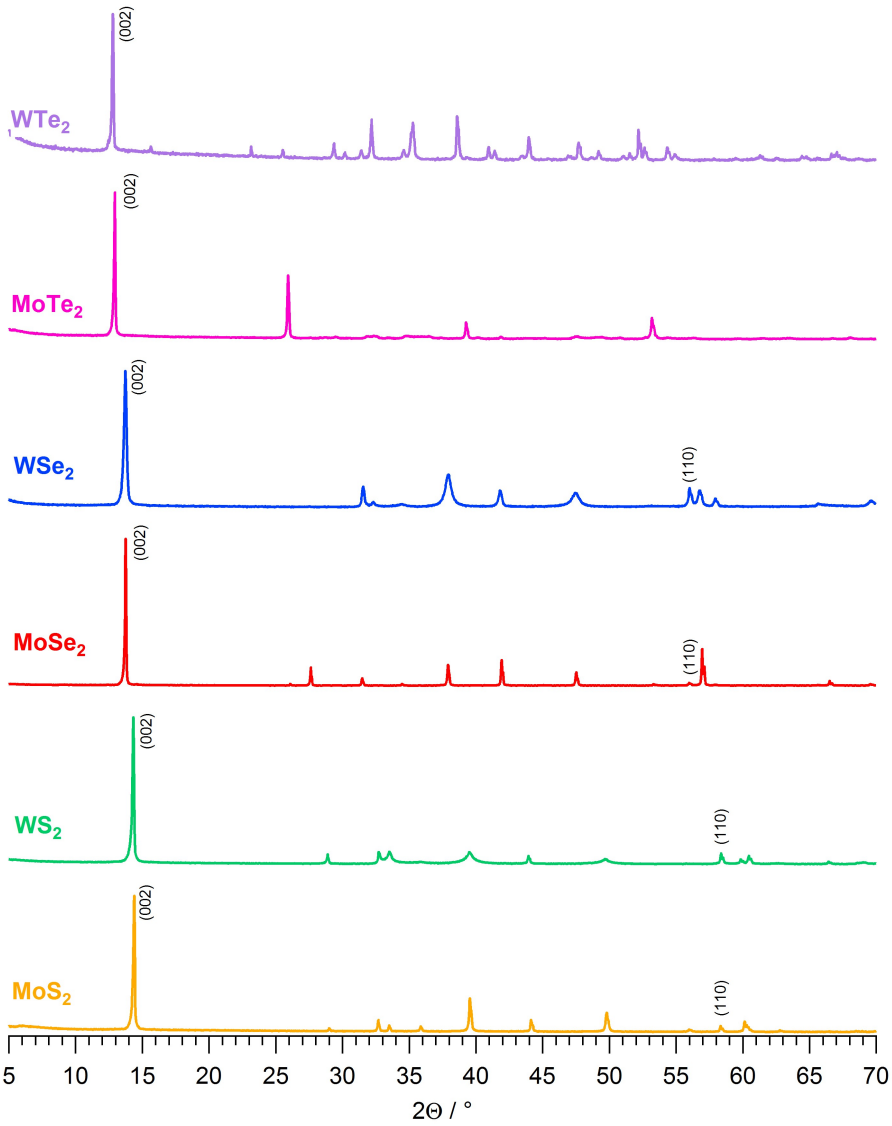

Figure S3: PXRD patterns for pristine (bulk) TMDCs of MX_2 composition (M = Mo, W; X = S, Se, Te).

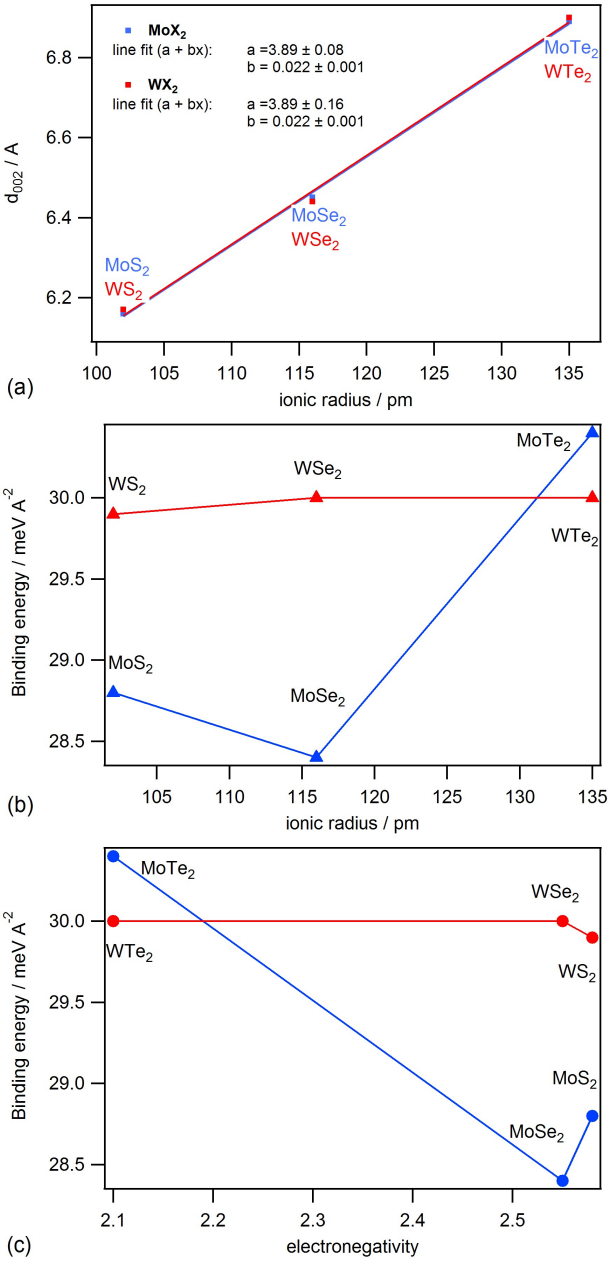

Figure S4: Correlation of (a) the position of (002) line with ionic radius of dichalcogenide atoms in MX_2 compounds; (b) rVV10 calculated binding energy [9] with ionic radius of dichalcogenide atoms in MX_2 compounds; (c) rVV10 calculated binding energy with electronegativity of dichalocogenide atoms.

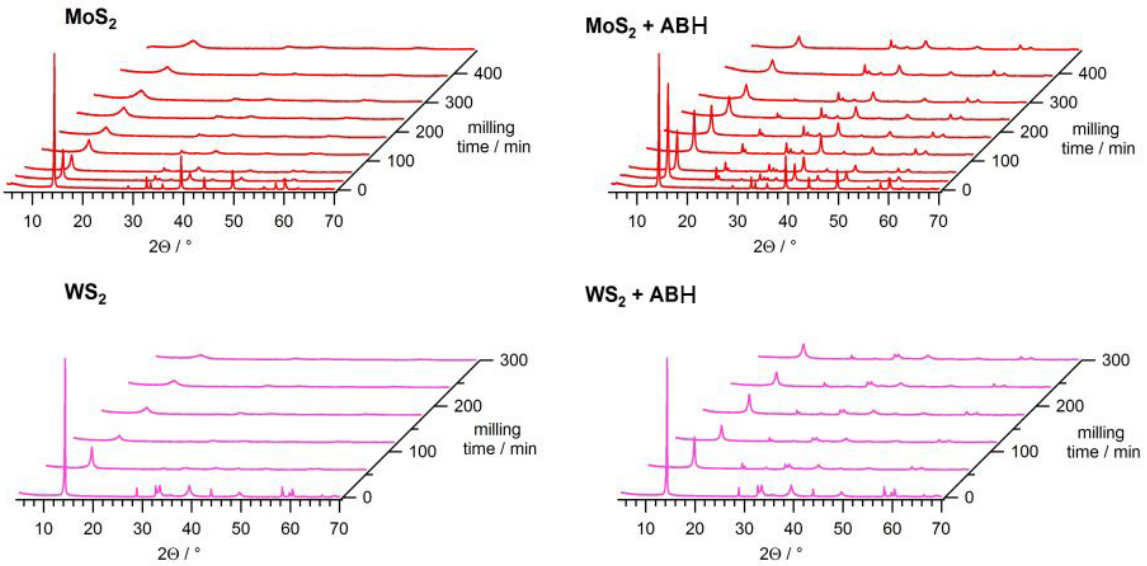

Figure S5: PXRD patterns for *ex-situ* monitored exfoliation of MoS2 and MoS2-ABH systems.

PXRD lines. On the other hand, PXRD patterns for MX_2 + ABH systems are characterised by well defined, narrow lines, which indicates a preservation of the crystal structure. The parameters of the most important PXRD lines, i.e. those corresponding to (002) and (110) reflections, are thus measured to obtain a better insight into behaviour of the considered systems (Figs. S7, S8, S12).

Table S3: The main XRD features.

	MX_2, initial				MX_2, B.M.				MX_2 + ABH, B.M.			
	d_{002}/Å	d_{110}/Å	$\frac{I_{002}}{I_{110}}$	phase	d_{002}/Å	d_{110}/Å	$\frac{I_{002}}{I_{110}}$	phase	d_{002}/Å	d_{110}/Å	$\frac{I_{002}}{I_{110}}$	phase
MoS_2	6.15	1.58	25.3	2H	6.28	1.57	9.4	2H	6.16	1.58	2.6	2H
$MoSe_2$	6.43	1.64	58.2	2H	6.70	1.63	4.3	2H	6.47	1.64	2.2	2H
$MoTe_2$	6.83	—	—	1T’	7.05	—	—	1T’	6.88	—	—	1T’
WS_2	6.18	1.58	14.8	2H	6.32	1.57	8.9	2H	6.25	1.58	1.0	2H
WSe_2	6.44	1.62	8.4	2H	6.61	1.62	8.6	2H	6.51	1.63	12.3	2H
WTe_2	6.82	—	—	Td	7.18	—	—	1T’	7.04	—	—	Td

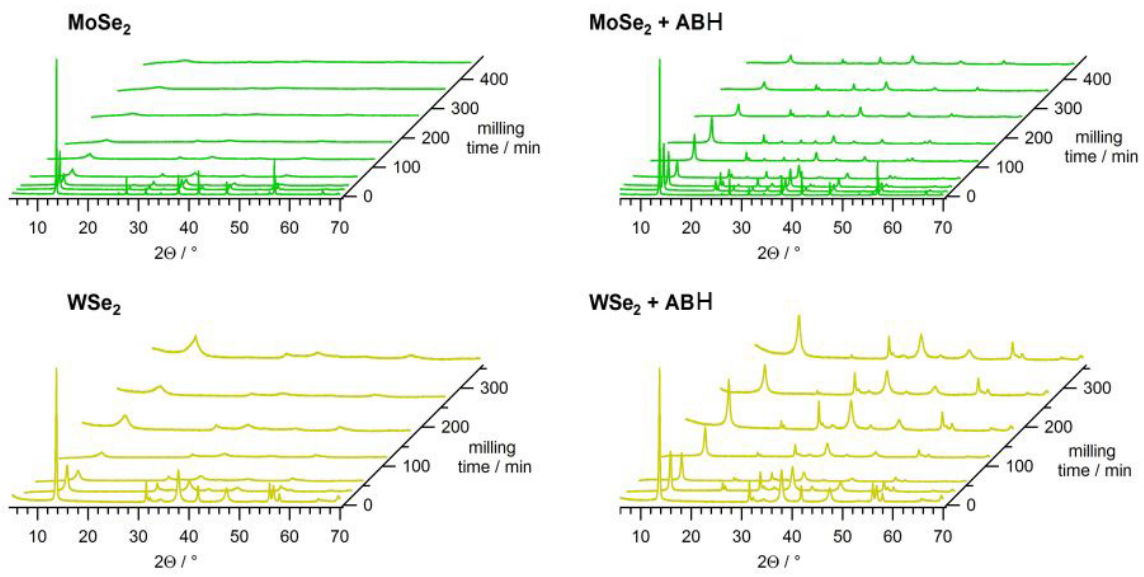

Figure S6: PXRD patterns for *ex-situ* monitored exfoliation of MoSe2 and MoSe2-ABH systems.

Table S4: Grain size as determined by DLS measurements vs. crystallite size, as obtained by Scherrer analysis of (002) and (110) XRD line, respectively.

System	d/nm	crystallite size /nm		System	d/nm	crystallite size /nm	
		(002)	(110)			(002)	(110)
MoS_2	203 ± 38	98	100	MoS_2 + ABH	179 ± 32	100	101
$MoSe_2$	208 ± 20	35	49	$MoSe_2$ + ABH	128 ± 8	136	158
$MoTe_2$	190 ± 27	42	—	$MoTe_2$ + ABH	213 ± 41	175	—
WS_2	120 ± 10	36	46	WS_2 + ABH	160 ± 26	90	255
WSe_2	219 ± 9	49	37	WSe_2 + ABH	254 ± 23	89	98
WTe_2	182 ± 30	89	—	WTe_2 + ABH	266 ± 8	106	—

Table S5: EDS analysis of MoSe2-ABH samples. The representative selenide samples were chosen according to IR spectra, Fig. S16, while EDS spectra were taken from regions as shown in Figs. . The difference of sum of the atomic % from 100 % is related to high content of oxygen (SEM-EDS analysis was done on more than 1 year old samples).

	atomic %				atom ratio			atomic %				atom ratio	
system	B	N	Mo	Se	B:N	Mo:Se	**system**	B	N	W	Se	B:N	W:
	37.6	4.9	3.2	5.8	7.7 : 1	1 : 1.8		29.7	8.4	0.5	1.0	3.5 : 1	1 :
MoSe2-ABH-180	30.15	8.5	—	—	3.5 : 1	—	WSe2-ABH-60	31.4	7.9	1.1	2.1	4 : 1	1 :
	31.0	9.1	—	—	3.4 : 1	—		30.0	2.6	5.3	9.3	11.5 : 1	1 :
	36.2	5.3	2.4	4.3	6.8 : 1	1 : 1.8		23.5	2.6	9.5	15.1	9.0 : 1	1 :
	—	—	25.1	43.4	—	1 : 1.7							
	—	—	23.8	42.8	—	1 : 1.8		—	—	23.6	44.2	—	1 :
MoSe2-ABH-450	—	—	25.5	45.8	—	1 : 1.8	WSe2-ABH-270	22.2	9.3	0.2	0.25	2.4 : 1	1 :
	—	—	26.4	46.7	—	1 : 1.8		11.3	0.9	16.3	27.5	12.0 : 1	1 :
	—	—	26.2	44.4	—	1 : 1.7							

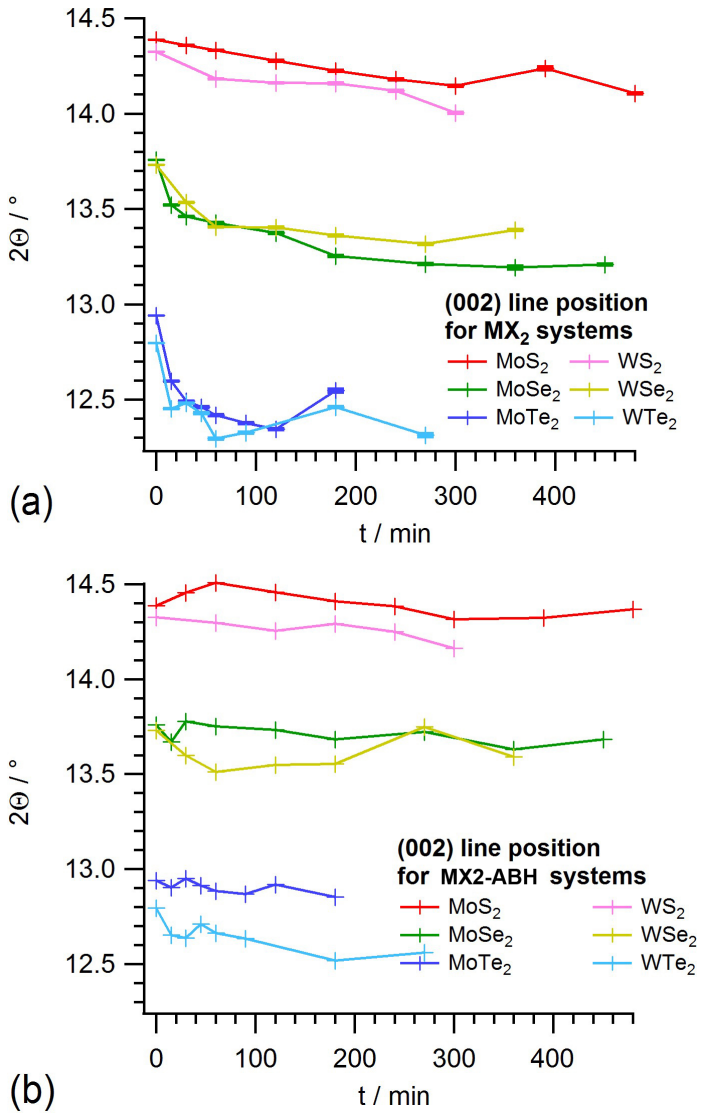

Figure S7: Position of the (002) line with respect of milling time.

Table S6: HER catalytic parameters of mechanically treated MoS_2 and WS_2 with borazane and pristine (control) sample.

Sample	**Treatment time** (min)	**Onset potential** (V vs. RHE)	**Tafel slope** (mV)	i_0 (10^{-6}Acm^{-2})
WS2-ABH	15	0.32794	117.93	1.65652
WS2-ABH	90	0.24499	100.68	3.68678
WS2-ABH	180	0.24386	111.47	6.49122
WS_2	180	0.29022	198.92	34.7553
MoS2-ABH	15	0.33057	133.43	3.33059
MoS2-ABH	90	0.24178	114.48	7.72708
MoS2-ABH	180	0.19483	88.1	6.1452
MoS_2	180	0.21837	146.85	32.5816

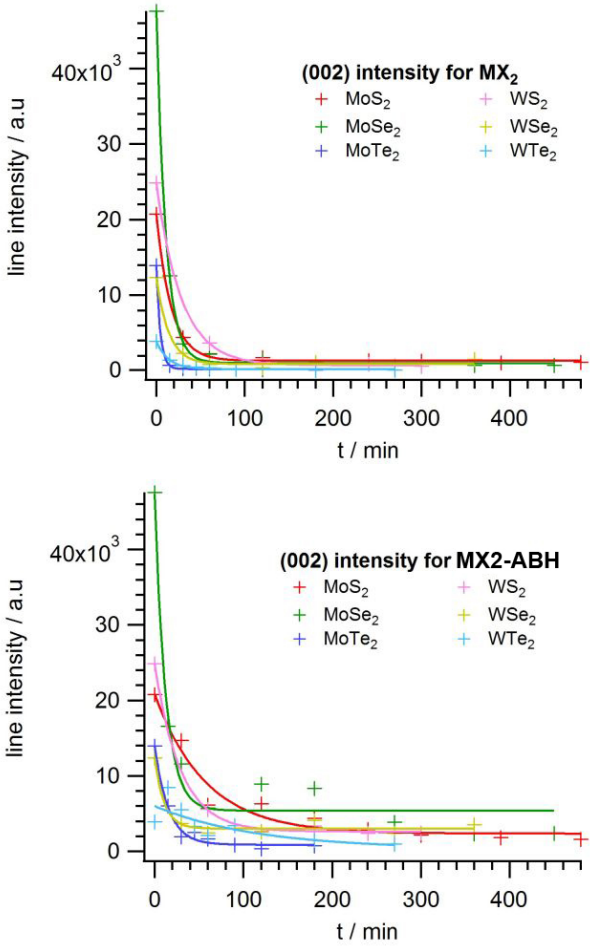

Figure S8: Intensity of the (002) line with respect of milling time.

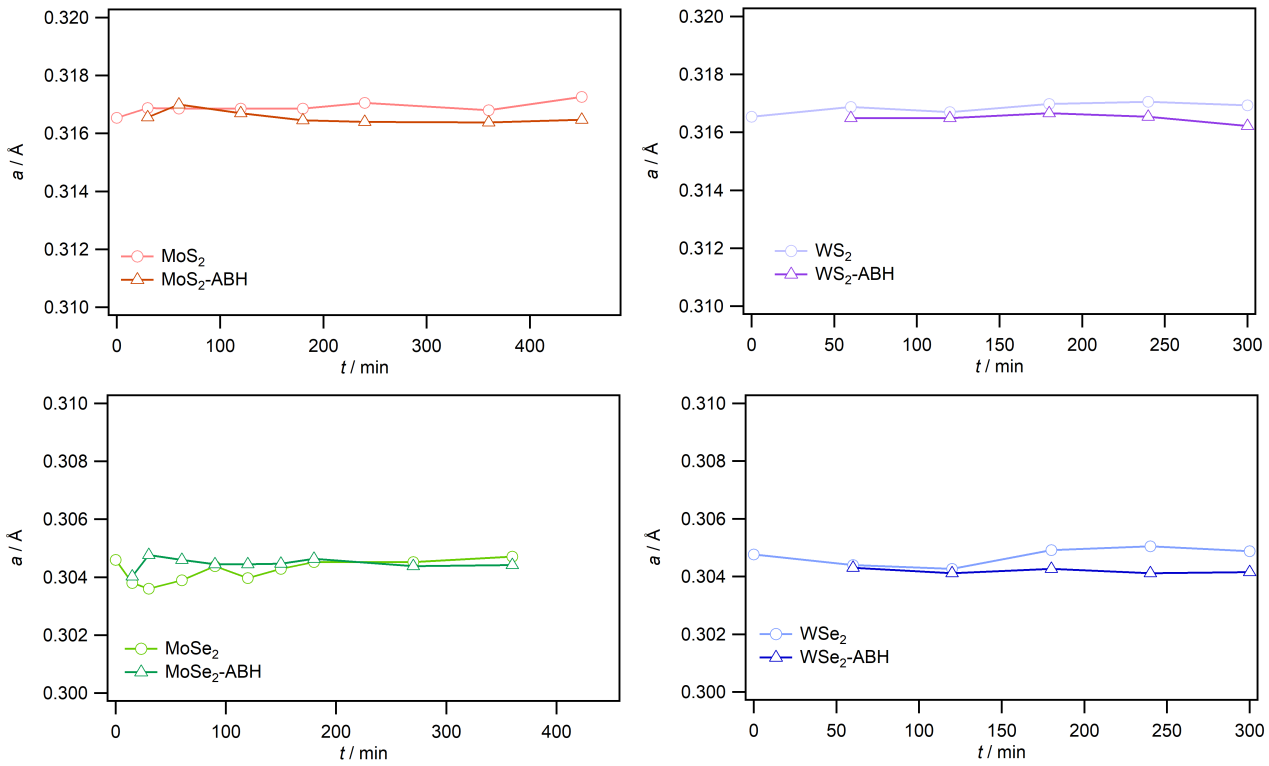

Figure S9: Cell parameter a, as calculated for hexagonal cell from (110) line

$$a = 1d_{hkl}$$

with respect of milling time.

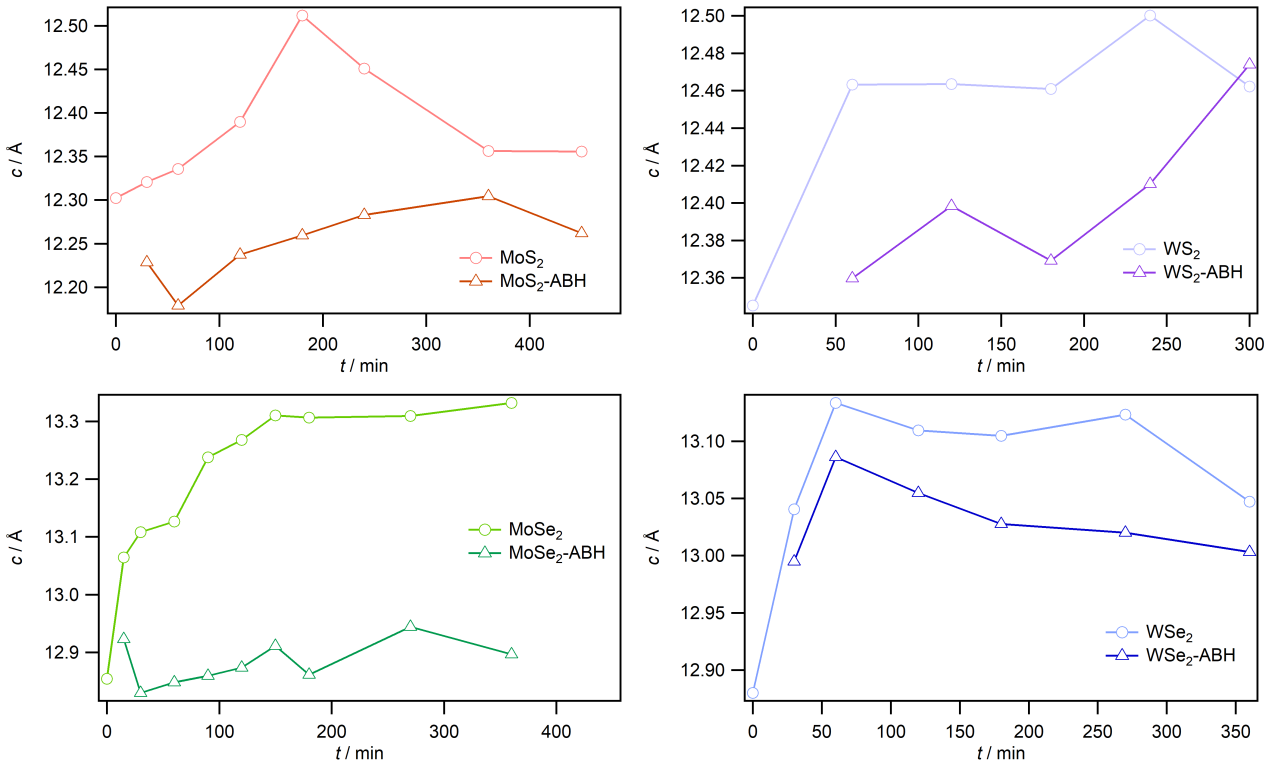

Figure S10: Cell parameter c, as calculated for hexagonal cell from (002) line

$$c = 2d_{hkl}$$

with respect of milling time.

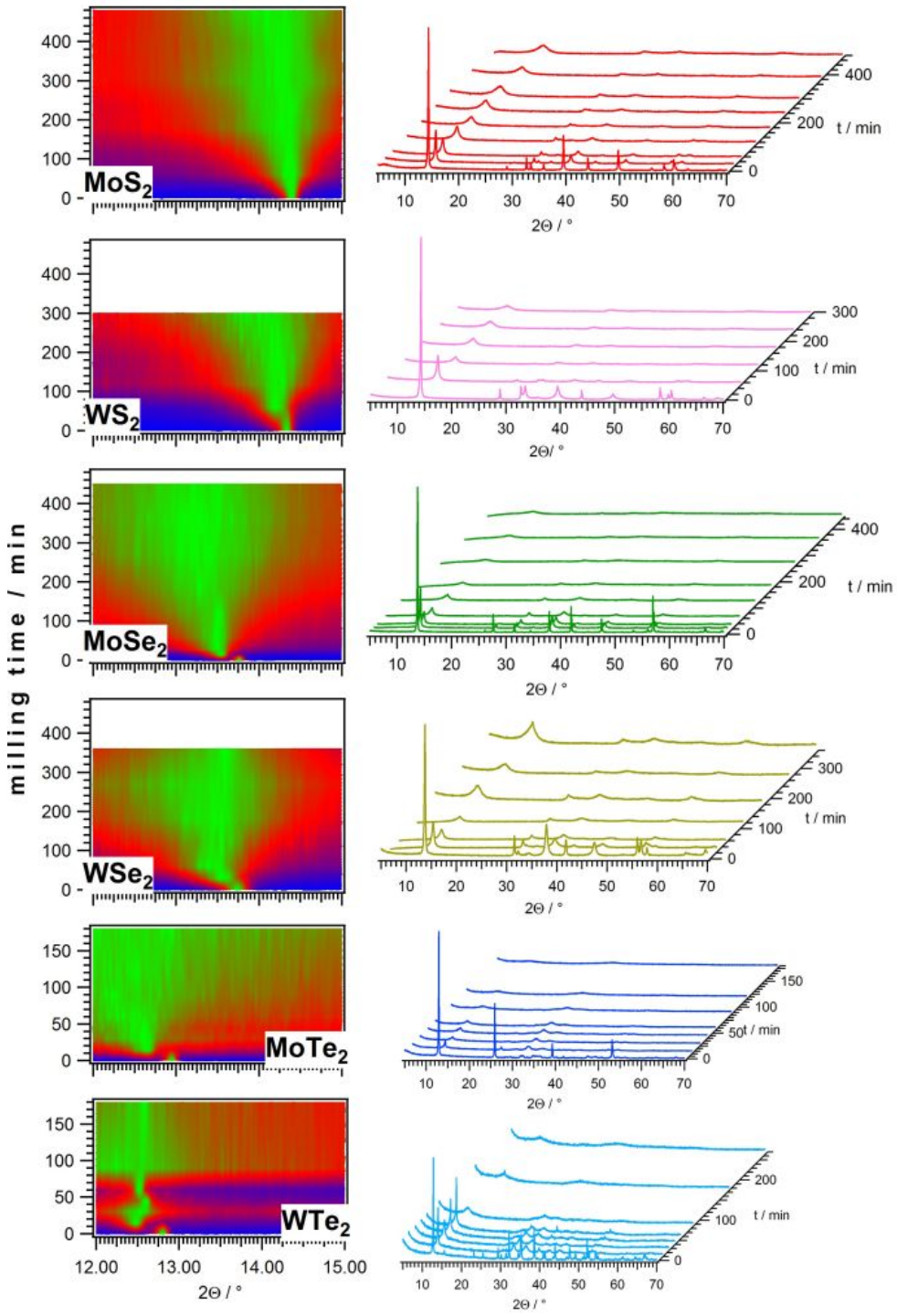

Figure S11: XRD patterns of pristine TMDCs with respect of milling time, and evolution of the (002) line during the milling. In order to accentuate the changes in postition and width, intensity of the line is set to 1 over the whole milling period.

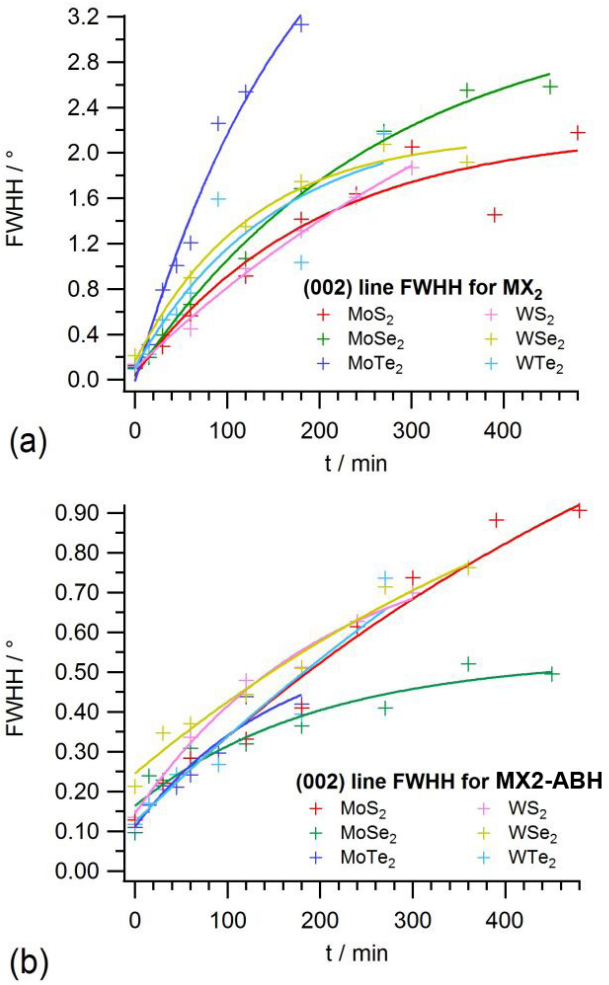

Figure S12: (002) line width with respect of milling time.

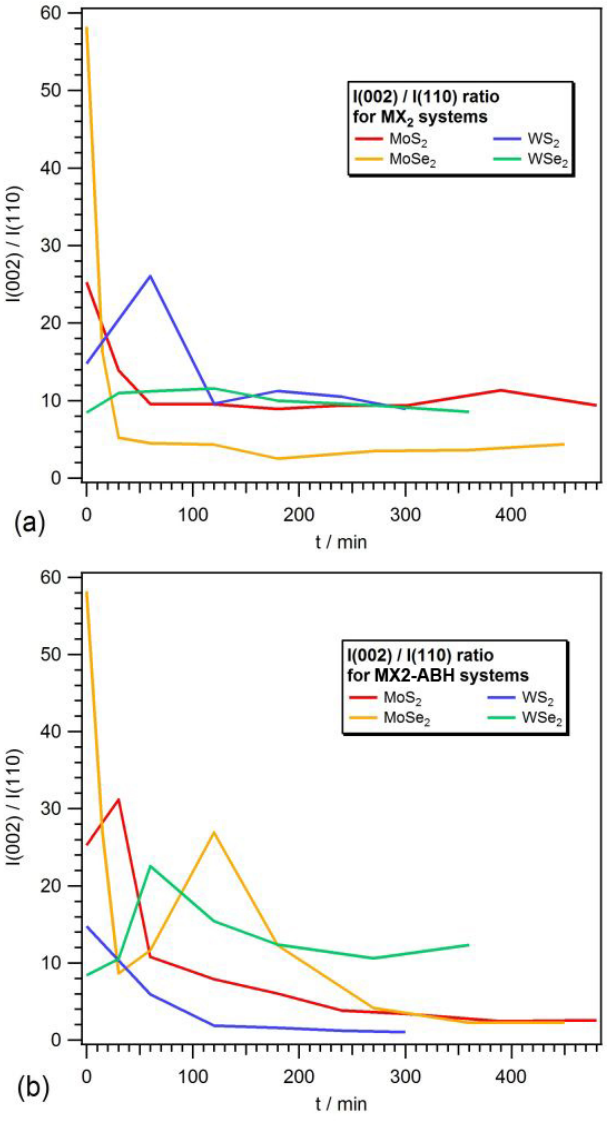

Figure S13: I_{002}/I_{110} ratio.

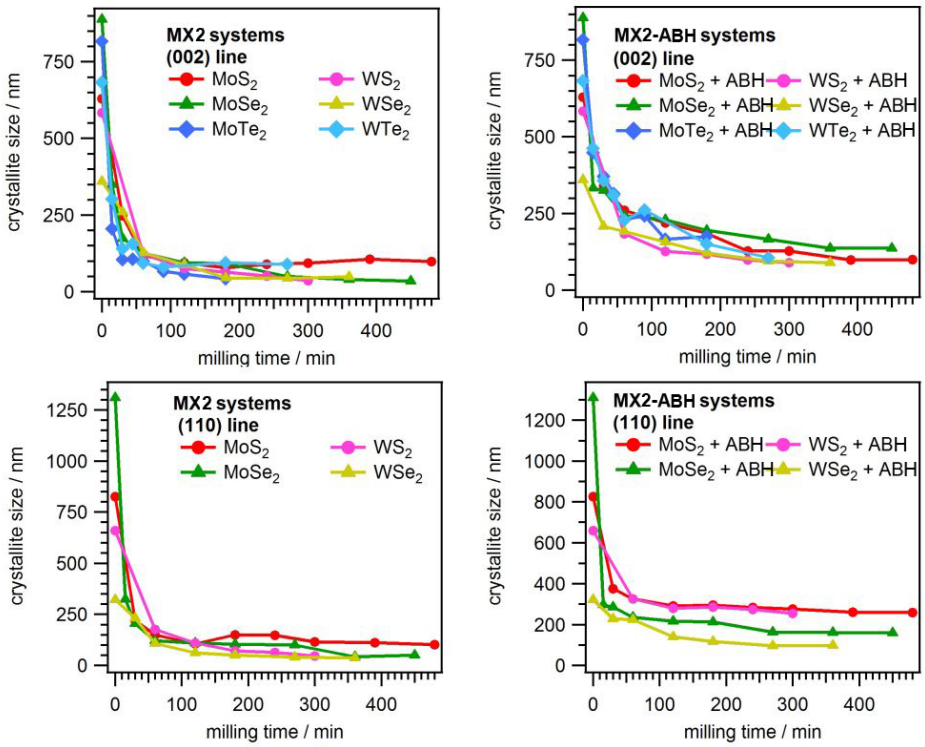

Figure S14: Crystallite size as determined by Scherrer analysis of (002) and (110) lines, respectively, vs. milling time.

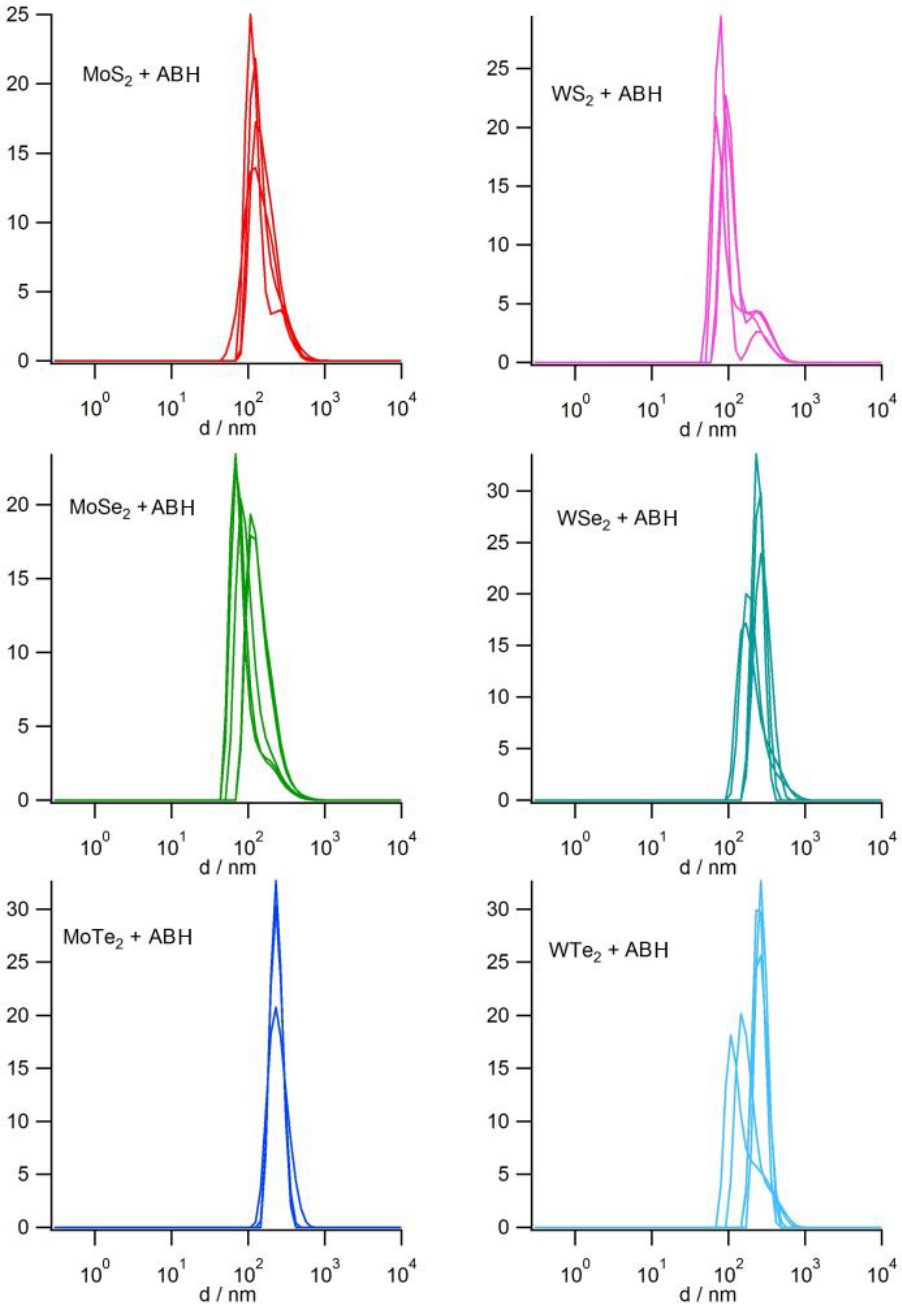

Figure S15: DLS measurements of the particle size distribution of final products of mechanochemical exfoliation.

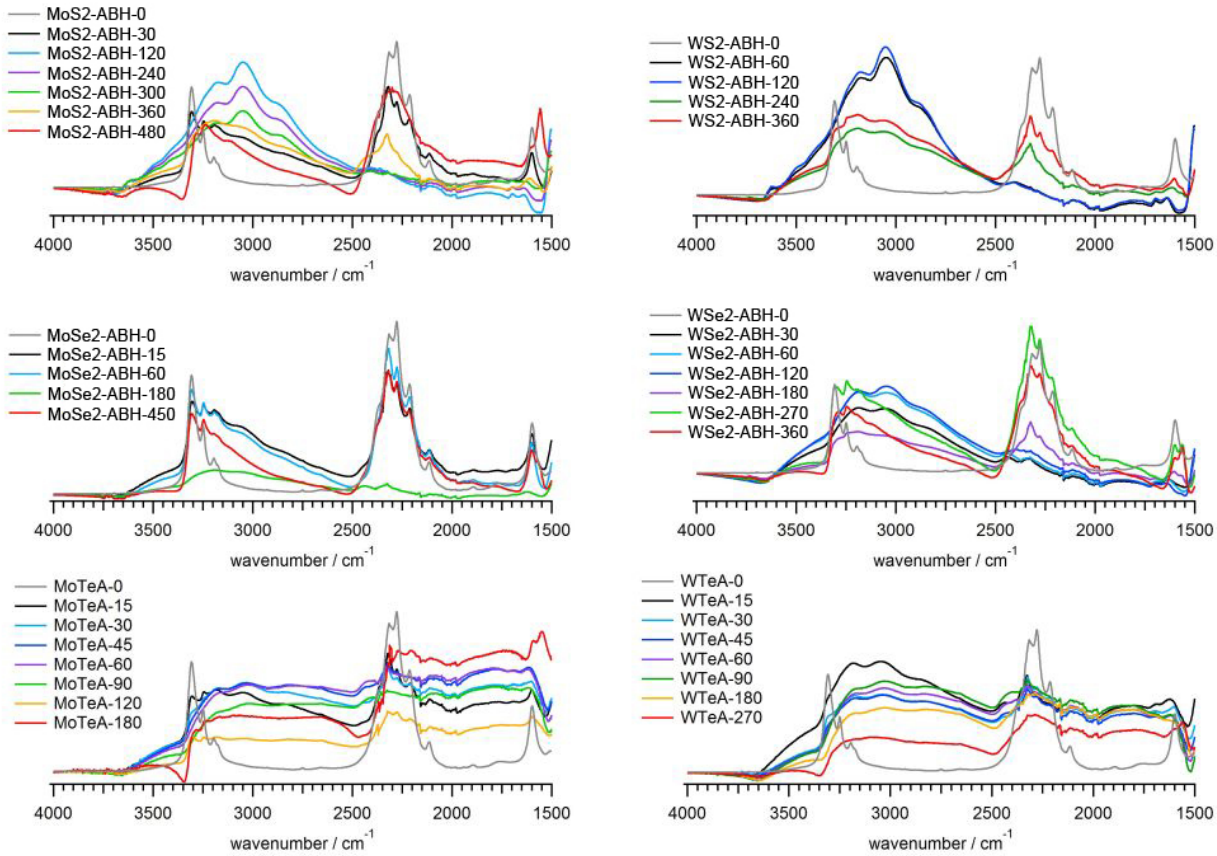

Figure S16: IR spectra of MX2-ABH systems with respect of the milling time.

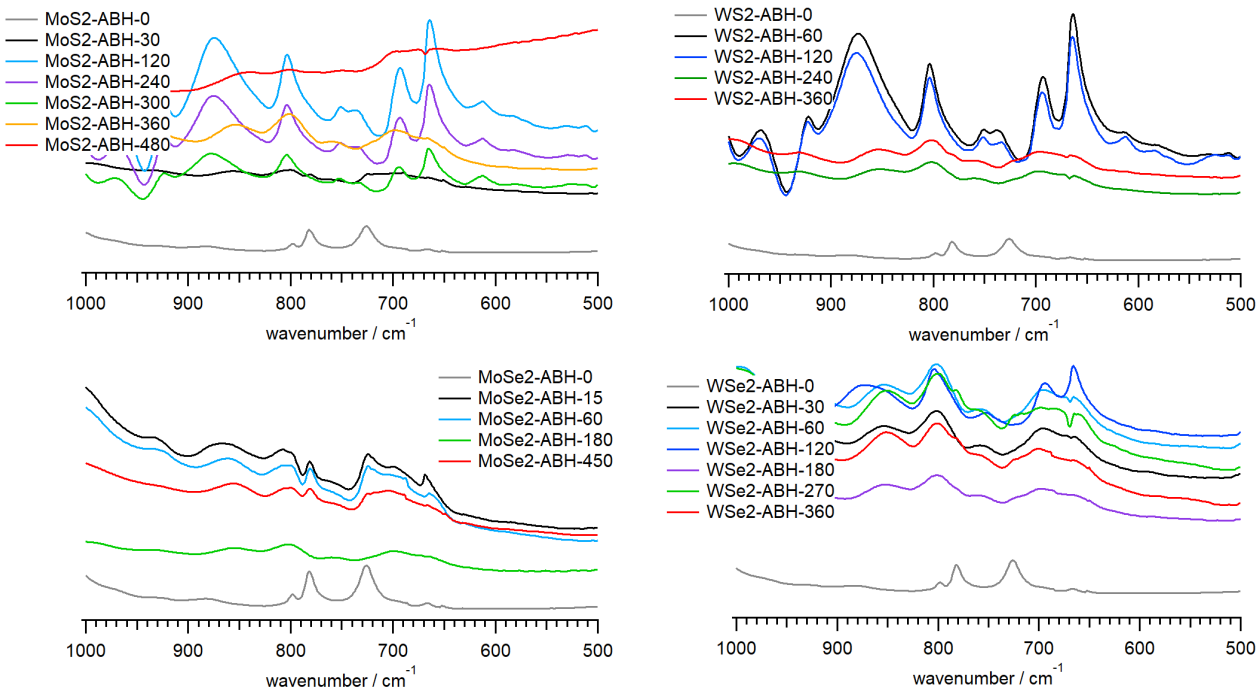

Figure S17: IR spectra of MX2-ABH systems in the ν(BN) region with respect of the milling time.

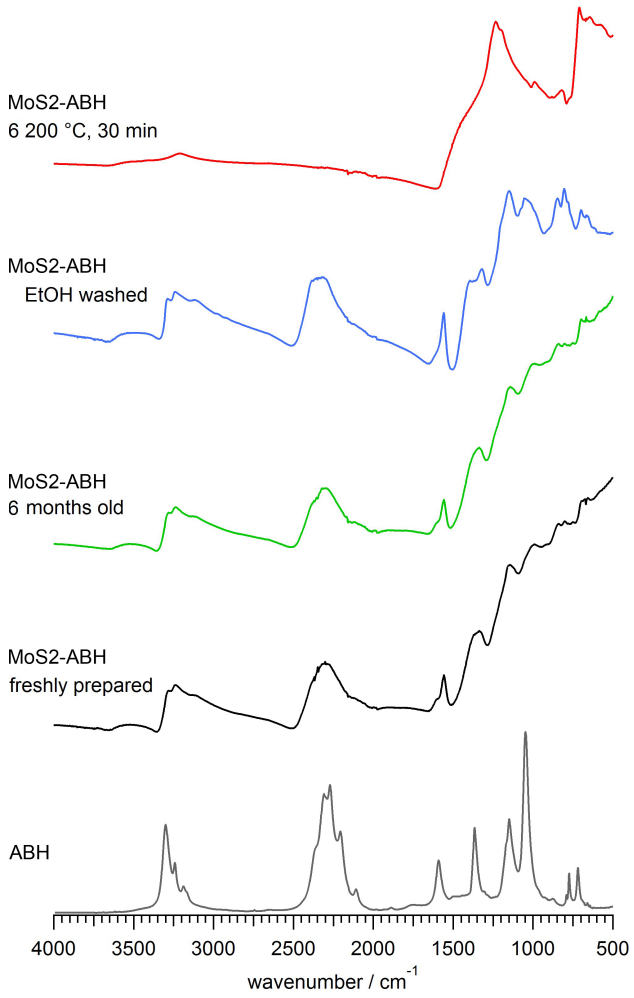

Figure S18: MoS2-ABH-480 system (480 min milled MoS_2 + ABH), compared to pristine ABH. IR spectra represent the fresh sample, measured immediatelly after milling, and the same system 6 months old, washed with EtOH (dispersed, sonicated over 15 min, centrifuged over 15 min, decanted and then 3× washed with EtOH), and heated at 200 °C over 30 min. It should be noted that EtOH is a relatively good solvent for ABH, and neat ABH readily sublimates under low vacuum.

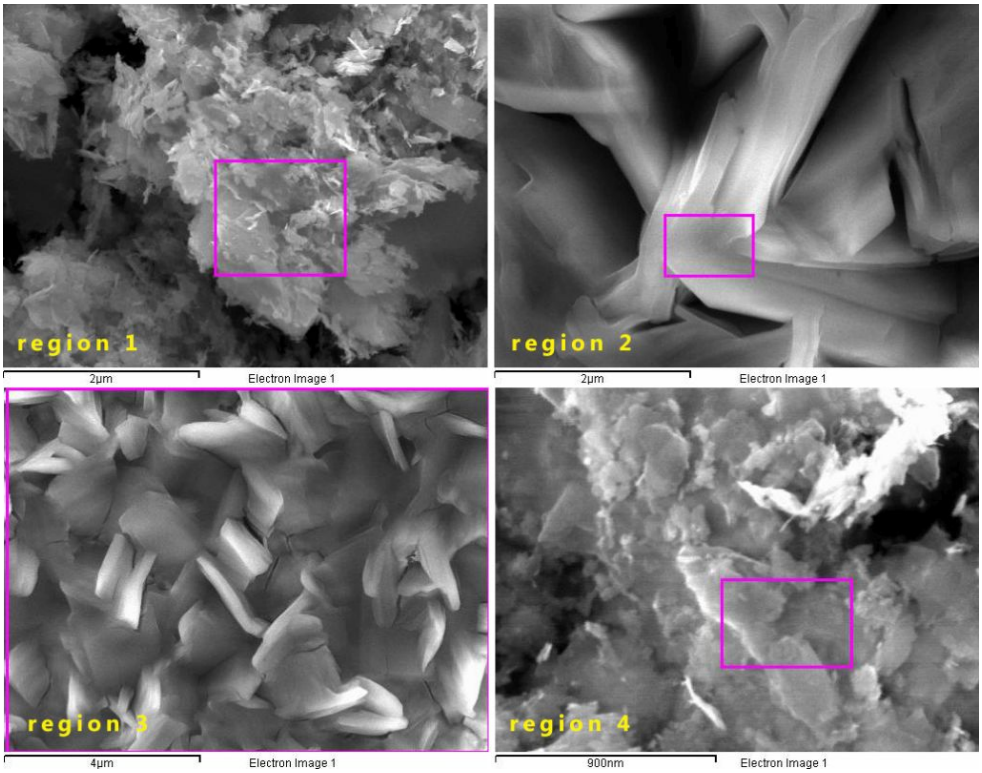

Figure S19: SEM of the regions from which EDS spectra of MoSe2-ABH-180 sample were taken.

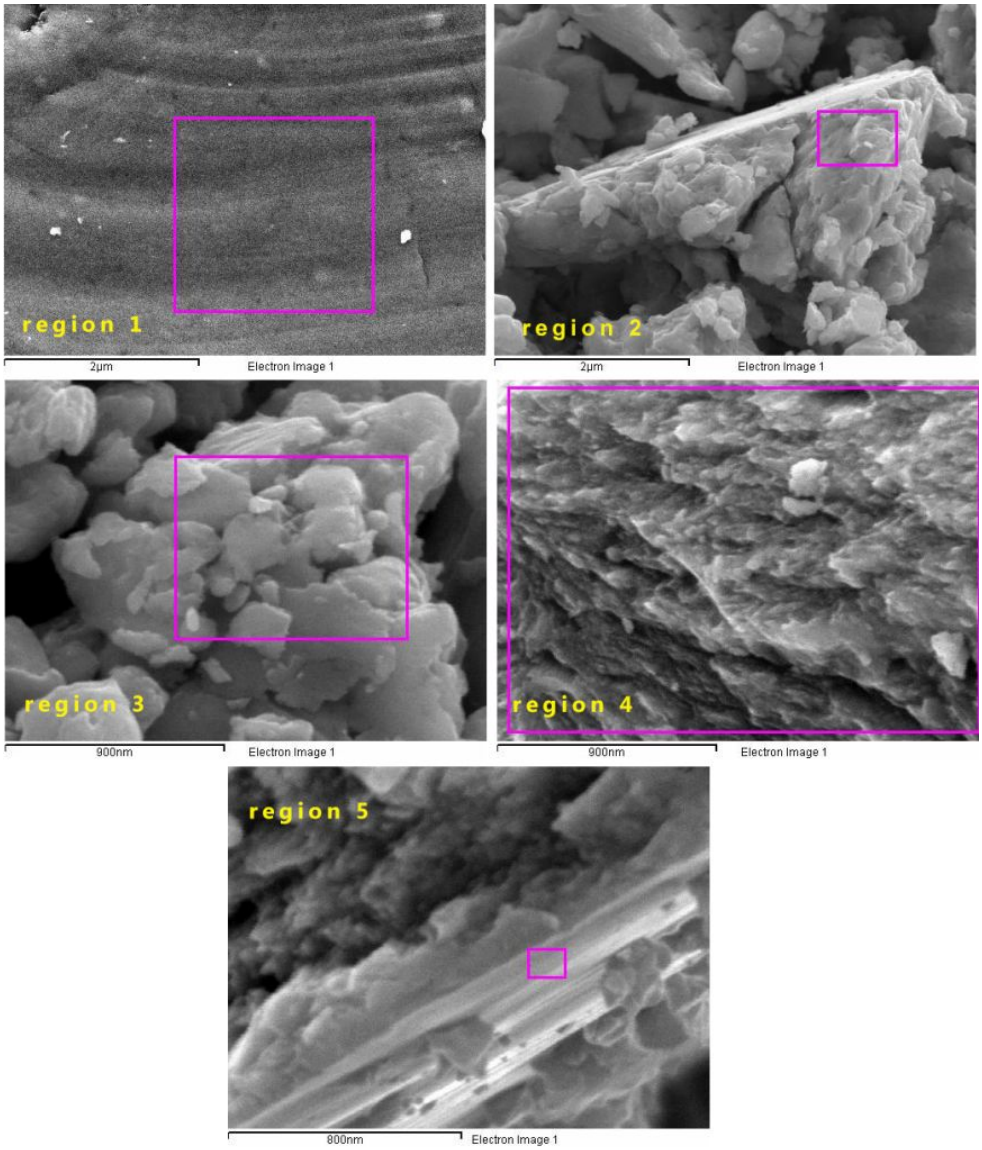

Figure S20: SEM of the regions from which EDS spectra of MoSe2-ABH-450 sample were taken.

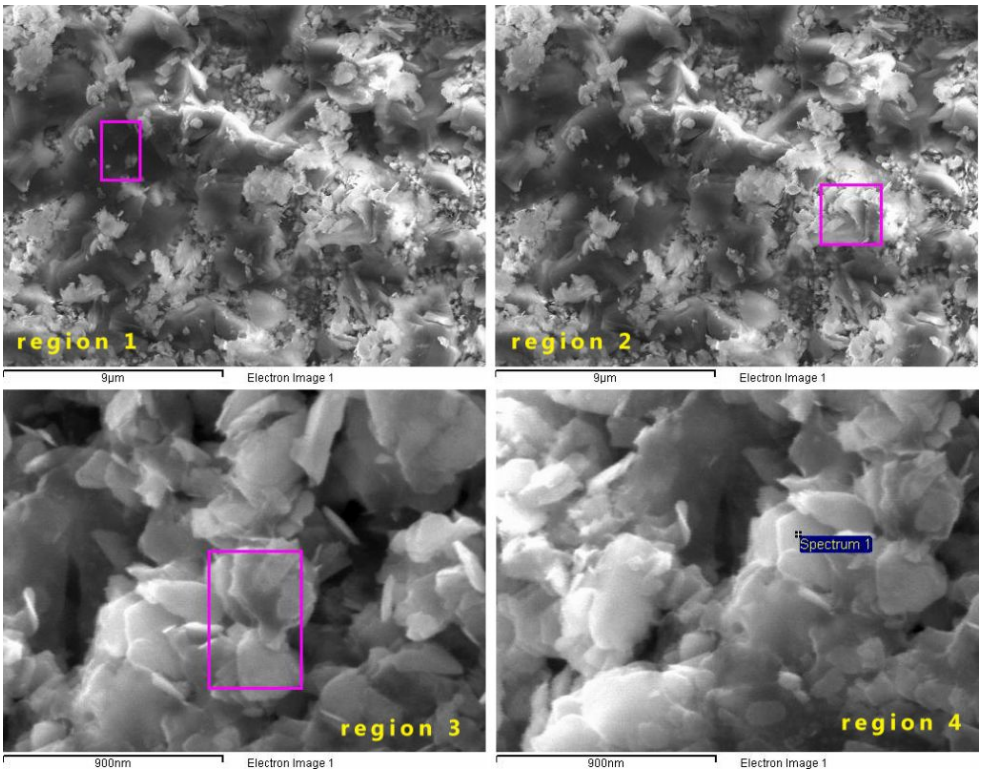

Figure S21: SEM of the regions from which EDS spectra of WSe2-ABH-60 sample were taken.

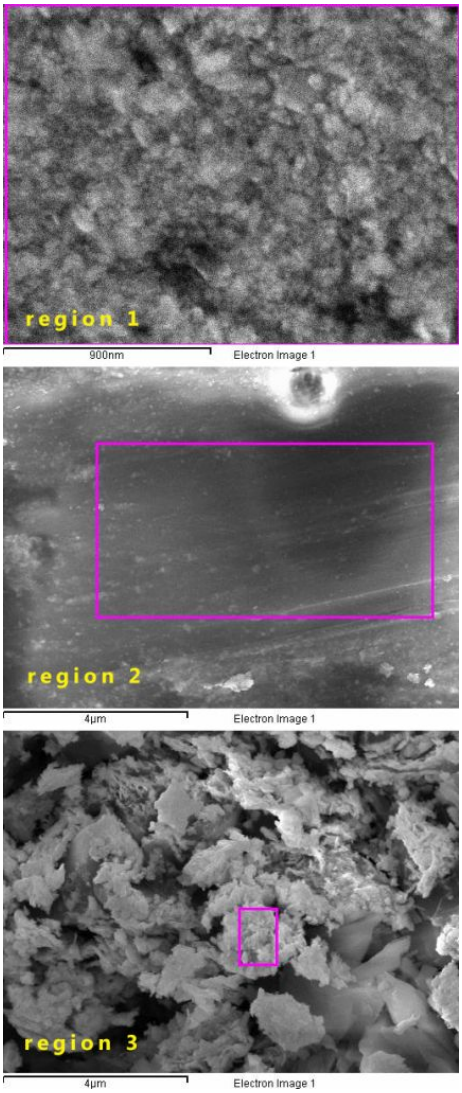

Figure S22: SEM of the regions from which EDS spectra of WSe2-ABH-270 sample were taken.

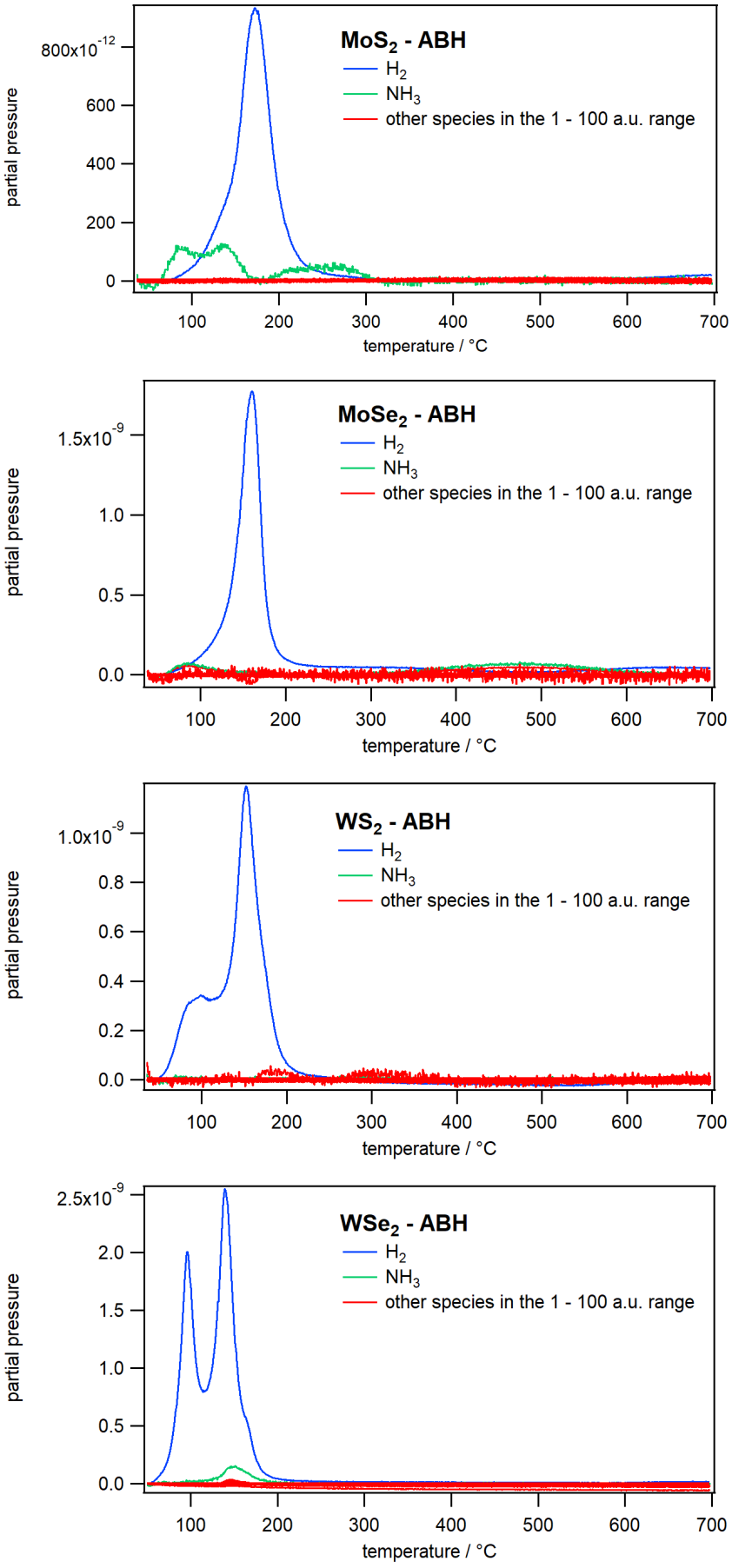

Figure S23: QMS curves showing temperature-dependant presence of gaseous products of decomposition of MX2-ABH systems in the $1 - 100$ mass range.

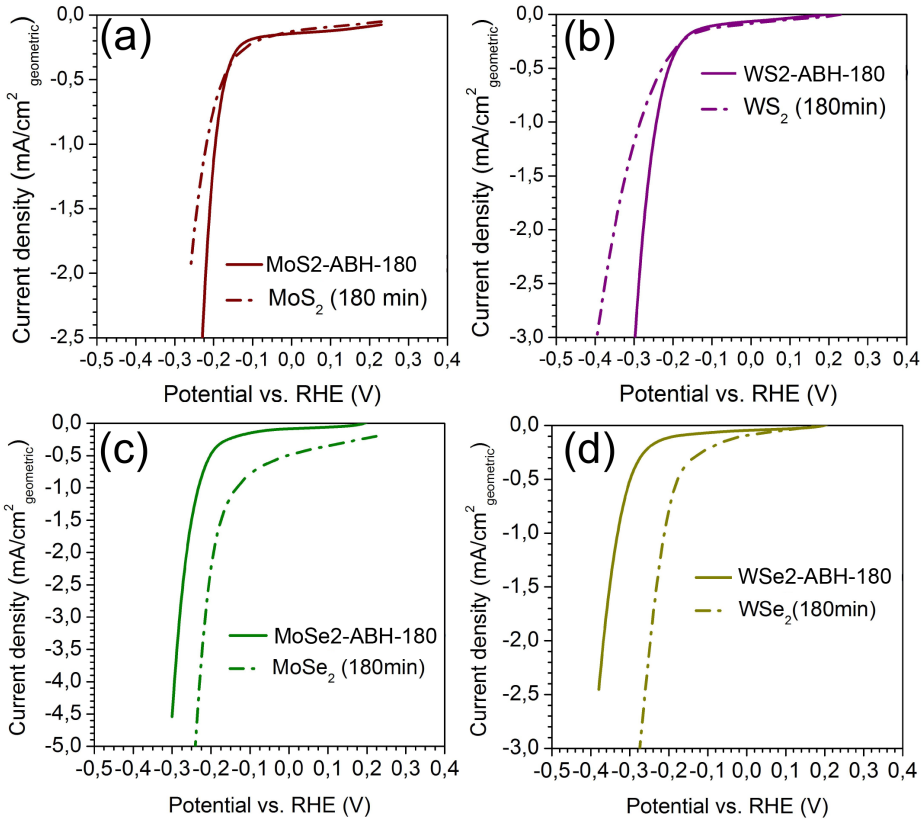

Figure S24: Polarization curves of tested MX_2 samples mechanically treated for 180 minutes (pristine and with borazane): (a) MoS_2, (b) WS_2, (c) $MoSe_2$ and (d) WSe_2; Scan rate: 5 mV/sec.

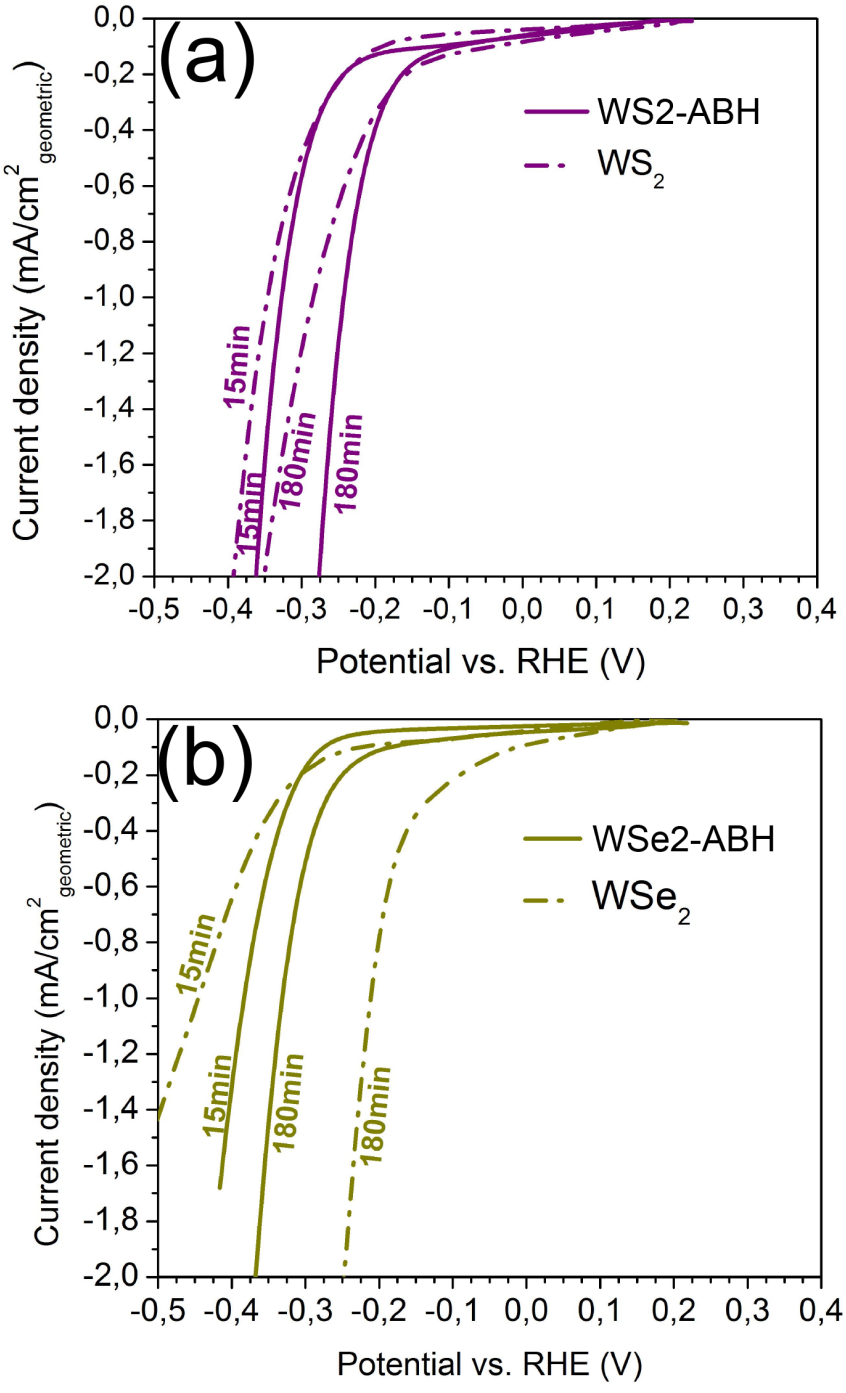

Figure S25: Polarization curves of tested (a) WS_2 and (b) WSe_2 samples mechanically treated for 15 and 180 min, pristine and with borazane; Scan rate: 5 mV/sec.

References

[1] B. E. GMBH CO KG, *Böhler N685 Extra Nichtro Stender Stahl Stainless Steel*, http://steirereisen.bisanz.me/wp-content/uploads/2014/02/N685DE.pdf, Accessed: 7. Feb. 2019.

[2] L. Liu, Z. Xiong, D. Hu, G. Wu and P. Chen, *Chem. Commun.*, 2013, **49**, 7890–7892.

[3] W. Chen, M. Schoenitz, T. S. Ward, R. N. Dave and E. L. Dreizin, *KONA Powder Particle J.*, 2005, 152–161.

[4] D. Maurice and T. H. Courtney, *Metallurg. Mater. Trans. A*, 1994, **25**, 147–158.

[5] D. Maurice and T. H. Courtney, *Metallurg. Mater. Trans. A*, 1996, **27**, 1981–1986.

[6] D. Maurice and T. H. Courtney, *Metallurg. Mater. Trans. A*, 1996, **27**, 1973–1979.

[7] T. W. Scharf and S. V. Prasad, *J. Mater. Sci.*, 2013, **48**, 511–531.

[8] C. Zhang, J. Tan, Y. Pan, X. Cai, X. Zou, H.-M. Cheng and B. Liu, *Nat. Sci. Rev.*, 2019, **7**, 324–332.

[9] N. Mounet, M. Gibertini, P. Schwaller, D. Campi, A. Merkys, A. Marrazzo, T. Sohier, I. Castelli, A. Cepellotti, G. Pizzi and N. Marzari, *Nature Nanotech.*, 2018, **13**, 246–252.